Journal of Hydrology 592 (2021) 125764

Contents lists available at ScienceDirect

Journal of Hydrology

journal homepage: www.elsevier.com/locate/jhydrol

Research papers

Coupled carbon-nitrogen cycling controls the transformation of dissolved inorganic carbon into dissolved organic carbon in karst aquatic systems

Haijuan Zhao [a,b], Yongjun Jiang [a,*], Qiong Xiao [b], Cheng Zhang [b], Hamid M. Behzad [a]

[a] Chongqing Key Laboratory of Karst Environment & School of Geographical Sciences, Southwest University, Chongqing 400715, China
[b] Key Laboratory of Karst Dynamics, MNR & Guangxi, Institute of Karst Geology, Chinese Academy of Geological Sciences, Guilin 541004, China

ARTICLE INFO

Keywords:
Coupled carbon-nitrogen cycling
Dissolved inorganic carbon
Nitrate
Dissolved organic carbon
Karst aquatic system
Lijiang River

ABSTRACT

The cycling of carbon (C) and nitrogen (N) in karst aquatic systems has been shown to be closely related, with coupled control of dissolved organic carbon (DOC) concentrations through the metabolic pathways of subaquatic communities. However, the coupled C—N cycling involving in the transformation of dissolved inorganic carbon (DIC) into DOC has not been well-explored. In this study, we chose the Lijiang River, a typical karst aquatic system in Southwest China as our study area and documented its diurnal and seasonal variations in terms of several hydrochemical and isotopic parameters to identify how to couple cycling for C and N. The results of the Bayesian stable isotope-mixing model showed that approximately 50% and 72% of the total DOC formed in summer and winter, respectively, represented autochthonous organic carbon in the Lijiang River. Diurnal monitoring results revealed that DIC and NO_3^- transformations were primarily controlled by metabolic processes (photosynthesis and respiration) of subaquatic communities, accompanying DOC formation, in the Lijiang River. The consumption of DIC and NO_3^- by aquatic photosynthesis was in the ratio of 9:1 (mol/mol) to produce autochthonous DOC, accompanying the enriched $\delta^{13}C_{DIC}$, $\delta^{15}N\text{-}NO_3^-$ and $\delta^{18}O\text{-}NO_3^-$, with a daily variation of 7.9‰, 10.6‰ and 11.2‰, respectively. On the diurnal scale, 6.2% of the total DIC and 7.1% of the total NO_3^- were consumed by metabolic processes of subaquatic communities and these values were consistent with their corresponding values on the interannual scale. However, the proportions of DIC and NO_3^- utilized in the dry season were higher than those in the wet season. Approximately 1.18×10^7 kg C/yr of DIC and 1.64×10^6 kg N/yr of NO_3^- were converted into organic matter by the aquatic photosynthesis, with 80% and 79% of the total DIC and NO_3^- consumption respectively occurring in the wet season. Furthermore, the coupled C—N cycling involving DIC and NO_3^- can promote the production of autochthonous DOC, constituting a relatively long-term natural C and N sinks in karst aquatic systems.

1. Introduction

Imbalances in global carbon (C) and nitrogen (N) budgets have become important environmental issues because of their inherent connection with contemporary climate change (Melnikov and O'Neill, 2006; Schlesinger, 2009; Zeng et al., 2019). C and N loading of aquatic systems is increasing worldwide due to intense human activities during the past decades (Peterson et al., 2001; Seitzinger et al., 2005; Xuan et al., 2019). In the 20th century alone, human activities have increased the delivery of N to rivers and streams from 34 to 64 Tg N/yr (Beusen et al., 2015). Of all N species, nitrate (NO_3^-) is the most dominant component (Beusen et al., 2015). The NO_3^- contamination of water is possibly the most widespread environmental problem in the world (Kendall et al., 2008; Xue et al., 2009), especially in karst water. Karstic aquifers are particularly sensitive and fragile to chemical contamination from anthropogenic activities due to their developed conduit networks and sinkholes (Jiang, 2013). A growing number of studies have found that the N from human activities has caused the coupled C—N cycling to be involved in the process of carbonate weathering, leading to an increased dissolved inorganic carbon (DIC) flux in karst aquatic systems (Jiang, 2013; Raymond et al., 2008; Zhao et al., 2020a). The higher DIC (half of which originates from soil/atm) from carbonate weathering and increased NO_3^- from human activities could fuel the growth of aquatic communities, which in turn could enhance the uptake of DIC and NO_3^-

* Corresponding author at: Chongqing Key Laboratory of Karst Environment & School of Geographical Sciences of Southwest University, Chongqing 400715, China.
E-mail address: jiangjyj@swu.edu.cn (Y. Jiang).

https://doi.org/10.1016/j.jhydrol.2020.125764
Received 28 July 2020; Received in revised form 6 November 2020; Accepted 9 November 2020
Available online 18 November 2020

(Liu et al., 2018; Zeng et al., 2019). Thus, the cycling of C and N in karst aquatic systems is closely related with a coupled control of organic carbon (OC) concentrations via assimilation process (Gruber and Galloway, 2008; Seitzinger et al., 2007; Trimmer et al., 2012; Zeng et al., 2019). However, little is known about the coupled C—N cycling in karst aquatic systems. In the coupled C—N cycling process, aquatic photosynthesis can consume DIC and NO_3^-, implying that DIC can be preserved in a relatively stable form by converting DIC into OC, while water quality can be enhanced by consuming NO_3^- (Liu et al., 2018; Nõges et al., 2016; Pedersen et al., 2013). Furthermore, the coupled C—N cycling could cause carbonate precipitation in karst aquatic systems. In this process, DIC and NO_3^- are transformed into organic matter and O_2 is released, which is in contrast with the traditional viewpoint of CO_2 release during carbonate precipitation (Jiang et al., 2013). The OC can be divided into particulate organic carbon (POC) and dissolved organic carbon (DOC) in aquatic systems and the latter accounts for ~60% of the total OC (Spitzy and Ittekkot, 1991). Moreover, the DOC is a key source of energy for driving functioning of the aquatic systems (Wen et al., 2020). Hence, it is important to obtain more insights into the coupled C—N cycling and the transformation of DIC into DOC in karst aquatic systems, which will shed more light on the stability of carbon sink associated with carbonate weathering and the improvement of water quality in these systems.

DIC evolution in karst aquatic systems includes CO_2 outgassing and DOC transformation, accompanied by the precipitation or dissolution of calcium carbonate (Jiang et al., 2020). NO_3^- evolution in aquatic systems includes N uptake by photosynthesis of subaquatic communities, organic nitrogen decomposition by respiration, and transformation of NO_3^- into N_2 by denitrification (Kendall et al., 2008). Thus, the coupled C—N cycling in karst aquatic systems involves the recognition of these processes. The respiration of subaquatic communities produces $\delta^{13}C$ depleted CO_2 with a $\delta^{13}C$ value close to that of organic matter, whereas photosynthetic uptake of DIC preferentially removes ^{12}C, leading to an enrichment of ^{13}C in the remaining DIC in water (Sun et al., 2015; Yang et al., 1996). Moreover, the elevated $\delta^{13}C_{DIC}$ by photosynthesis can be enhanced by CO_2 outgassing due to preferential loss of ^{12}C relative to ^{13}C (Jiang et al., 2013; Telmer and Veizer, 1999). The denitrification of bacteria and photosynthesis of subaquatic communities generally preferentially uses lighter isotopes, which would lead to the enrichment of heavier isotopes in the remaining NO_3^-. The denitrification results in $\delta^{15}N$ and $\delta^{18}O$ values of the remaining NO_3^- increasing with a relationship of 1.3:1 to 2.1:1 (Lee et al., 2008; Xue et al., 2009), whereas the assimilation of NO_3^- during photosynthesis results in $\delta^{15}N$ and $\delta^{18}O$ values of the remaining NO_3^- increasing with a relationship of 1:1 (Granger et al., 2004). Meanwhile, autochthonous DOC produced by aquatic photosynthesis has significant differences in the $\delta^{13}C$ and C/N values with allochthonous DOC. Generally, the $\delta^{13}C$ and C/N values for phytoplankton (PP) and macrophytes (MP) are −42‰ to −24‰ and 5 to 8 (Kendall et al., 2001), and −28‰ to −18‰ and 10 to 30 (Kendall et al., 2001), respectively, whereas the $\delta^{13}C$ and C/N values for soil organic matter (SOM), C3 plants, and C4 plants are −25‰ to −22‰ and 10 to13 (Goñi et al., 2003), −32‰ to −22‰ and >15 (Kendall et al., 2001), and −16‰ to −9‰ and 15 to >50 (Kendall et al., 2001), respectively. Therefore, hydrochemical parameters (e.g. Ca^{2+}, DIC, NO_3^-, DO, DOC, POC and C/N) and isotopes (e.g. $\delta^{13}C_{DIC}$, $\delta^{13}C_{DOC}$, $\delta^{15}N\text{-}NO_3^-$ and $\delta^{18}O\text{-}NO_3^-$) are powerful tools to study the coupled C—N cycling and the transformation of DIC into DOC in karst aquatic systems.

In this study, a typical karst aquatic system – the Lijiang River in Southwest China – was chosen as the study area and seasonal and diurnal variations in C and N were investigated. The hydrogeochemical and isotopic data (DIC, NO_3^-, NH_4^+, DON, DOC, POC, DO, $\delta^{13}C_{DIC}$, $\delta^{13}C_{DOC}$, $\delta^{15}N\text{-}NO_3^-$, and $\delta^{18}O\text{-}NO_3^-$) were analyzed to better understand the coupled C—N cycling in karst aquatic systems. Thus, the new aspect addressed here is to identify how to couple cycling for C and N in the typical karst aquatic system.

2. Study area

The study was conducted in the Lijiang River, which is located in the northeast of Guangxi Province, the center of the well-known karst regions of Southwest China. The river basin is situated between the coordinates of 24°16′-26°21′N and 109°45′-111°02′ E with a drainage area of 5039.7 km^2 and a length of 164 km, in a region of mid-subtropical monsoon climate (Fig. S1). This area is strongly affected by East Asian monsoon and South Asian monsoon, with 80% of annual precipitation occurring between March and August. The mean annual temperature and precipitation are ~19 °C and ~2000 mm, respectively. The vegetation in the drainage basin is characterized by tropical evergreen forests dominated by subtropical coniferous forest, broadleaf forest, bamboo forest and grassland. The aquatic vegetation in the Lijiang River is characterized by submerged C3-macrophytes dominated by *Vallisneria spiralis*, *Ceratophyllum demersum* and *Hydrilla verticillate*. Phytoplankton in the Lijiang River mainly includes *Chlorophyta*, *Bacillariophyta* and *Cyanophyta*. The lithology of the upper part of the catchment is chiefly Silurian granites, Ordovician-Cambrian shales, and mud rocks intercalated with carbonate rocks (Zhao et al., 2020a). In contrast, the lithology of the mid-lower parts is dominated by Devonian carbonate rocks (Zhao et al., 2020a). Thus, karst landscape is well-developed in the mid-lower reaches of the Lijiang River.

3. Methods

3.1. Sampling and analysis

3.1.1. Seasonal sampling and analysis

Twelve sampling sites (M1-M3 in the upper reaches, M4-M6 in the middle reaches, M7 and M8 in the lower reaches, and T1-T4 of four main tributaries) were selected along the Lijiang River (Fig. S1). To capture the influence of storm-water runoff and discharge in the river, two sampling campaigns were conducted in the wet season (August 2017) and in the dry season (December 2017). In addition, monthly monitoring of hydrochemistry was performed at site M8 during January–December 2017. All water samples were filtered through glass-fiber filters (precombusted GF/F filters, 0.7 μm pore size) into polyethylene bottles. POC samples were extracted by filtering river water through the baked 0.7 um glass-fiber filters. Samples of the potential DOC sources were also collected: including ten samples of representative aquatic plant samples (*Hydrilla verticillate*, *Vallisineria spiralis*, *Ceratophyllum demersum* and *Spirogyra*) and five phytoplankton samples from the Lijiang River. We collected phytoplankton using 1 m vertical tows through the water column using a 64 μm plankton net and used the protocol developed by Hamilton et al. (2005) to partition fine particulate matter into predominantly phytoplankton and detrital components by centrifugation in colloidal silica (Ludox TM-50; density 1.40 g/cm^3). In addition, six soil samples were collected from a depth of 0–30 cm under the corresponding dominant plants (*Castanopsis fargesii*, *Loropetalum chinense*, *Pinus massoniana*, *Pinus elliottii*, eucalypt and bamboo). Soil samples were dried in the oven at 45 °C for two days, then ground to pass a sieve (mesh 200). Plant samples were rinsed with distilled water and dried in an oven at 50 °C for two days. After drying, the plant samples were ground into a powder form with diameters <150 μm to ensure homogeneity. All samples were stored at a temperature <4 °C in the laboratory before measurement.

Water temperature (T), pH and DO were measured on site using a portable water-quality analyzer (YSI 6920, USA). HCO_3^- (CO_3^{2-}) concentrations were determined in situ by titration with an alkalinity test kit with resolution of 0.1 mmol/L. Concentrations of major cations (K^+, Na^+, Ca^{2+} and Mg^{2+}) and anions (NO_3^-, Cl^- and SO_4^{2-}) were measured by inductively coupled plasma-optical emission spectrometry (ICP-OES; resolution of 0.01 mg/L) and ion chromatography (IC; resolution of 0.01 mg/L), respectively. Ammonium (NH_4^+) concentrations were measured spectrophotometrically using the Berthelot reaction with a

detection limit of 0.02 mg/L. DOC and dissolved nitrogen (DN) concentrations were analyzed on an Analytik Jena N/C Multi3100 instrument with resolution of 0.01 mg/L. Dissolved organic nitrogen (DON) concentrations were calculated using the difference between DN and NO_3^- concentrations. POC concentrations were determined using an elemental analyzer (Vario Isotope Cube-Isoprime, Elementar company) with resolution of 0.01 mg/L. $\delta^{13}C_{DOC}$ values were determined using an elemental analyzer coupled to an isotope-ratio mass spectrometer (iso TOC Cube-Isoprime 100, Elementar company) while $\delta^{13}C_{DIC}$ values were analyzed using a GasBench II-IRMS system (Thermo Fisher Scientific, USA). For soil and plant samples, the elemental analyzer (Vario Isotope Cube-Isoprime, Elementar company) was used to determine the stable C isotope compositions and C/N ratios. All C/N values reported were atomic (at.) ratios. The results of $\delta^{13}C$ analysis were reported relative to the V-PDB standard and the overall experimental accuracy for $\delta^{13}C$ measurements was ±0.2‰. The $\delta^{18}O$-H_2O values were determined with a liquid water stable isotope analyzer (LWIA-24-d, Los Gatos Research, USA). $\delta^{15}N$-NO_3^- and $\delta^{18}O$-NO_3^- values were measured using an elemental analyzer interfaced with a MAT 253 isotope-ratio mass spectrometer (Thermo Fisher Scientific, USA). The results of $\delta^{15}N$ were reported relative to N_2 in the atmosphere and $\delta^{18}O$ were reported to the Vienna Standard Mean Ocean Water. The analytical error was typically ±0.2‰ for $\delta^{15}N$-NO_3^-, ±0.3‰ for $\delta^{18}O$-NO_3^- and ±0.2‰ for $\delta^{18}O$-H_2O.

The pCO_2 of water were calculated based on hydrochemical data, including water temperature, pH and concentrations of seven major ions (K^+, Na^+, Ca^{2+}, Mg^{2+}, Cl^-, SO_4^{2-} and HCO_3^-), by using the modified program WATSPEC (Wigley, 1977) (Eq. (1)).

$$pCO_2 = \frac{(HCO_3^-)(H^+)}{K_H K_1} \quad (1)$$

where K_H and K_1 represent the temperature-dependent Henry's Law constant for CO_2 and dissociation constant for H_2CO_3 in water, respectively.

3.1.2. Diurnal sampling and analysis

A 48-h sampling campaign was conducted during sunny days from October 30 to November 1, 2017 at 2-h intervals to evaluate the existence and magnitude of in-river diel variations at site M6 (Fig. S2) in the middle reaches of the Lijiang River, in which there are a large number of aquatic plants, including *Hydrilla verticillate*, *Vallisineria spiralis* and *Spirogyra*. The water temperature, pH and DO at this site were measured in situ at 15-min intervals using the multi-parameter meter (YSI 6920, USA). Resolutions of T, pH and DO were 0.01 °C, 0.1 pH units and 0.01 mg/L, respectively. Discrete river-water samples (DIC, NO_3^-, DOC, $\delta^{13}C_{DIC}$, $\delta^{15}N$-NO_3^-, $\delta^{18}O$-NO_3^- and $\delta^{18}O$-H_2O) were collected every two hours from October 30 through November 1, 2017. All water samples collection and analysis were completely consistent with the above-described procedure.

3.2. Seasonal data calculations and statistical analysis

3.2.1. Quantification of the contributions of DOC sources in the Lijiang River

To quantify the contributions of different DOC sources in the Lijiang River, the Bayesian stable isotope-mixing model was used. This model has been implemented using a "SIAR" (Stable Isotope Analysis in R) software package and can be expressed as follows (Parnell et al., 2010):

$$X_{ij} = \sum_{k=1}^{k} P_k(S_{jk} + C_{jk}) + \varepsilon_{ij} \quad (2)$$

$$S_{jk} \sim N(\mu_{jk}, \omega_{jk}^2)$$

$$C_{jk} \sim N(\lambda_{jk}, \tau_{jk}^2)$$

$$\varepsilon_{ij} \sim N(0, \sigma_j^2)$$

where X_{ij} is the isotope value j of water sample I; P_k is the proportional contribution of source k, which is estimated using the Bayesian model; S_{jk} is the source value k of isotope j, C_{jk} is the fractionation factor of isotope j on source k, and ε_{ij} is the residual error representing additional unquantified variations between individual samples.

To estimate the proportional contribution of DOC sources, only one isotope (j = 1) ($\delta^{13}C$) and three major potential DOC sources (Soil organic matter, phytoplankton and macrophytes) were considered in this study. 11 samples of plant leaves and stems collected in the Lijiang River basin had C/N ratios from 24.7 to 107.7 (Table S1), which were significantly different from the DOC/DON ratios of the river water (as mentioned in Section 4.2) and other potential DOC sources (as mentioned in Section 4.1). Therefore, terrestrial plants were not considered as the potential DOC sources in this study. The values of three major potential DOC sources were −23.1‰ ± 1.7‰, −25.0‰ ± 1.5‰ and −30.5‰ ± 2.1‰ for SOM, MP and PP, respectively (as mentioned in Section 4.1). For $\delta^{13}C$ values of DOC leachates from MP and PP, we used the $\delta^{13}C$ of MP and PP biomass, as we did not have direct measurement of the $\delta^{13}C$ values of DOC leachates from MP and PP. We acknowledge that this is only a first-order approximation of the $\delta^{13}C$ values of DOC leachates from MP and PP in this study and look forward to further refining this model endpoint when better data become available. The corresponding experiments for determining enrichment factors are out of the scope of this study. Thus, we assumed $C_{jk} = 0$ in Eq. (2).

3.2.2. Estimation of autochthonous DOC concentrations in the Lijiang River

Autochthonous DOC concentrations (C_{ADOC}) were estimated using Eq. (3),

$$C_{ADOC} = C_{DOC} \times A_m \quad (3)$$

where Am (based on the discussion in Section 5.1.), representing the contribution of autochthonous DOC, is the sum of the contributions of macrophytes and phytoplankton to DOC; C_{DOC} is the concentration of DOC.

3.2.3. Estimation of annual DIC and NO_3^- loss during metabolism of subaquatic communities

The annual DIC (F_{ADIC} (kg C/yr)) and NO_3^- (F_{ANO3} (kg N/yr)) loss by metabolism of subaquatic communities were calculated using the monthly DOC concentration (C_{DOC}), the contributions of macrophytes (A_{MP}) and phytoplankton (A_{PP}) and the monthly average discharge (Q_m) at the mouth of the Lijiang River, and the C/N ratios of macrophytes (R_{MP}) and phytoplankton (R_{PP}) as follows:

$$F_{ADIC} = \sum_{m}(C_{DOC}/12) \times (A_{MP} + A_{PP}) \times Q_m \times 12 \quad (4)$$

$$F_{ANO3} = \sum_{m}(C_{DOC}/12) \times (A_{MP}/R_{MP} + A_{PP}/R_{PP}) \times Q_m \times 14 \quad (5)$$

where F_{ADIC} and F_{ANO3} are given by the sum of monthly losses of DIC and NO_3^- due to metabolism of subaquatic communities in one hydrological year; Q_m is the monthly average discharge at the river mouth (Table S2), where m = 1, 2, 3…, 12. C_{DOC} denotes the monthly DOC concentration at the river mouth (Table S2). A_{mp} and A_{PP} are the contributions of macrophytes and phytoplankton to DOC, respectively (A_{mp} and A_{PP} were set as 23% and 27% during the wet season (March to August), respectively, and as 35% and 37% during the dry season (September to February), respectively). These values were obtained based on the discussion in Section 5.1. R_{MP} (mean = 11) and R_{PP} (mean = 6.4) represent the C/N ratios of macrophytes and phytoplankton, respectively (as mentioned in Section 4.1). However, this approach of estimation of

annual DIC and NO_3^- loss during metabolism of subaquatic communities did not consider that: (i) both DOC and POC are produced by the photosynthetic use of DIC by subaquatic communities; (ii) only a fraction of DIC is converted into DOC and most of it is incorporated into biomass.

3.3. Diurnal data processing and analysis

3.3.1. Determining DIC losses by CO_2 evasion

Carbon dioxide fluxes across the water–air interface can be calculated using a molecular diffusion model (Raymond et al., 2012),

$$\mathrm{Fa} = \mathrm{k} \times (p\mathrm{CO_{2water}} - p\mathrm{CO_{2air}}) \quad (6)$$

where Fa is the CO_2 evasion flux (mg/m^2·h) between water and air, k is the gas-transfer velocity (cm/h), and $p\mathrm{CO_{2water}} - p\mathrm{CO_{2air}}$ is the CO_2-concentration gradient between water and air (ppmv). Atmospheric CO_2 concentration was found to be 445 ppmv at a location 1.5 m above the stream surface (Pu et al., 2016). We calculated k using the temperature-dependent Schmidt number (Sc_T) for fresh water (Raymond et al., 2012).

3.3.2. Determining changes in DIC concentrations due to calcite precipitation or dissolution

As described by Jiang et al. (2020), carbonate precipitation reduces Ca^{2+} and HCO_3^- concentrations by a ratio of 1:2 (mol/mol) and simultaneously releases 1 mol of CO_2 (aq.) into solution, and conversely, carbonate dissolution increases Ca^{2+} and HCO_3^- concentrations by a ratio of 1:2 (mol/mol) and removes 1 mol of CO_2 (aq.) from the solution. Thus, the DIC loss by calcite precipitation or gain by calcite dissolution were calculated from the changes in Ca^{2+} concentrations and the molar ratio of Ca^{2+} and HCO_3^-.

3.3.3. Determining changes in DIC concentrations due to metabolism of subaquatic communities

Biologically generated DIC was quantified using the gross primary productivity (GPP) and respiration rates (ER) with respect to DO concentrations. The net ecosystem production (NEP) represents the difference between GPP and ER (Demars et al., 2015; Odum, 1956; Pu et al., 2016),

$$\mathrm{NEP(dt)} = \frac{\mathrm{DO_t} - \mathrm{DO_{t-1}}}{\mathrm{dt}} - \mathrm{Kr} \times \Delta\mathrm{DO} + \mathrm{G} \quad (7)$$

where dt represents a time step, $\mathrm{DO_t} - \mathrm{DO_{t-1}}$ (mg/L) is the change in oxygen concentration between recording intervals, ΔDO is the excess oxygen (ΔDO = 100% saturation DO − measured DO value), Kr is the reaeration coefficient, which is the rate of exchange of oxygen with the ambient atmosphere, and G is the river water–groundwater exchange that affects DO concentration at the sampling site (Marcarelli et al., 2010; Pu et al., 2016). We assume that G is negligible because the monitoring point (M6) is mainly supplied by surface water. The concentration of completely (100%) saturated DO (mg/L) at a given water temperature was calculated as described elsewhere (Rice and Association, 2012). The DIC affected by the metabolism of subaquatic communities can be estimated based on the DIC:O_2 molar stoichiometry (1:1) (del Giorgio and Williams, 2015).

3.3.4. Estimation of magnitudes of $\delta^{13}C_{DIC}$ variations

The contributions of different processes to variations in $\delta^{13}C_{DIC}$ were calculated using a time-stepping chemical/isotope (^{12}C and ^{13}C) mass balance model (Jiang et al., 2020; Tobias and Bohlke, 2011) based on the DIC loss/gain. The model requires (i) the initial $\delta^{13}C$ values of the DIC from the Lijiang River (−9.4‰ (the minimum value of $\delta^{13}C_{DIC}$ before sunrise)), PP (−30.5‰), MP (−25.0‰), and atmospheric CO_2 (−9.9‰ (obtaining from Jiang et al. (2020))and (ii) fractionation factors, 0.9989 and 1.002 at 20 °C for air–water exchange (for CO_2(aq)–CO_2(gas) equilibrium) and gas dissolution, respectively (Tobias and Bohlke, 2011), 1.0007 for carbonate precipitation ($HCO_3^-/CaCO_3$) (Tobias and Bohlke, 2011), 0.9830 and 1.0000 (assuming no fractionation during the respiration of OC to CO_2) for photosynthesis and respiration by both PP and MP, respectively (Mook, 2006). Previous studies have found that the aqueous DIC species came to chemical and isotopic equilibrium within each time step, $CaCO_3$ precipitated in isotopic equilibrium with DIC, and transfer of CO_2 between air and water had a small kinetic fractionation associated with diffusion near the interface (Tobias and Bohlke, 2011; Zhang et al., 1995). A detailed description of this model can be found in Tobias and Bohlke (2011) and Jiang et al. (2020).

3.3.5. Determining changes in NO_3^- concentrations due to metabolism in subaquatic communities

NO_3^- loss (F_{NO3} (mol)) due to metabolism of subaquatic communities can be calculated using Eq. (8),

$$F_{\mathrm{NO3}} = \left(\left[\mathrm{NO_3^-}\right]_{MAX(0)} - \left[\mathrm{NO_3^-}\right]_{\mathrm{t}}\right) \Big/ 62 \times \mathrm{Q} \quad (8)$$

where $[NO_3^-]_{MAX(0)}$ (8.68 mg/L) is the maximum concentration of NO_3^- before sunrise, $[NO_3^-]_t$ is the concentration of NO_3^- at time t, and Q is discharge at site M6.

3.3.6. Estimation of magnitudes of $\delta^{15}N$-NO_3^- and $\delta^{18}O$-NO_3^- variations

The changes in $\delta^{15}N$-NO_3^- and $\delta^{18}O$-NO_3^- values during the assimilation process can be described with a Rayleigh-distillation model (Mariotti et al., 1981). This process is expressed by

$$\delta_t = \delta_0 + \varepsilon ln\left(\frac{NO_{3\,t}^-}{NO_{3\,0}^-}\right) \quad (9)$$

where δ_t is the $\delta^{15}N$ or $\delta^{18}O$ value of the residual NO_3^- at time t, δ_0 is the initial $\delta^{15}N$ or $\delta^{18}O$ value of the NO_3^-, and ε is the enrichment factor. $NO_{3\,t}^-$ and $NO_{3\,0}^-$ represent the NO_3^- concentrations of residual NO_3^- and initial NO_3^- during the assimilation, respectively. δ_0 and $NO_{3\,0}^-$ were assigned to be the minimum $\delta^{15}N$-NO_3^- value (3.9‰) and the maximum NO_3^- concentration (8.68 mg/L) before sunrise at M6, respectively. The enrichment factors for $\delta^{15}N$ (−7.67‰) and $\delta^{18}O$ (−7.55‰) were obtained from Fig. S3.

4. Results

4.1. $\delta^{13}C$ and C/N of macrophytes, phytoplankton and soil organic matter

As shown in Table 1, compared to the soil organic matter, macrophytes and phytoplankton in the Lijiang River showed depleted $\delta^{13}C$ values and lower C/N values. The $\delta^{13}C$ and C/N values of macrophytes and phytoplankton ranged from −27.5‰ to −23.2‰ with an average value of −25.0‰ ± 1.5‰ and 9.8 to 12.7 with an average value of 11.0 ± 1.0, and −33.9‰ to −28.8‰ with an average value of −30.5‰ ± 2.1‰ and 5.3 to 7.6 with a mean value of 6.4 ± 0.9, respectively. In contrast, the $\delta^{13}C$ and C/N values of the soil organic matter varied from −25.2‰ to −21.2‰ and 12.5 to 13.7, with a mean value of −23.1‰ ± 1.7‰ and 13.2 ± 0.4, respectively.

4.2. Seasonal and spatial variations of hydrogeochemical parameters and isotopes of the water in the Lijiang River

During the seasonal sampling periods, the NH_4^+ concentrations of the river water at most sampling sites were lower than the detection limit (0.02 mg/L), and the detectable NH_4^+ concentrations accounted for <5% of the total dissolved inorganic nitrogen (DIN). There were insignificant seasonal variations ($p > 0.05$) in NO_3^- concentrations of the water samples collected from the main river and tributaries, ranging from 1.10

Table 1
$\delta^{13}C$ values and C/N ratios of macrophytes, phytoplankton and soil organic matter.

Sample type	$\delta^{13}C$ (‰)	C/N (at.)
Macrophytes		
Hydrilla verticillate in M3	−23.2	12.0
Hydrilla verticillate in M4	−23.3	10.3
Hydrilla verticillate in M6	−24.9	10.7
Vallisineria spiralis in T1	−23.8	12.2
Vallisineria spiralis in M6	−23.5	12.7
Vallisineria spiralis in M8	−25.8	10.3
Ceratophyllum demersum in M4	−26.7	10.1
Ceratophyllum demersum in M8	−25.4	11.0
Spirogyra in M5	−27.5	11.0
Spirogyra in M8	−26.2	9.8
Phytoplankton		
Phytoplankton in M3	−30.2	7.6
Phytoplankton in M4	−30.0	6.8
Phytoplankton in M6	−28.8	5.3
Phytoplankton in M8	−29.7	5.9
Phytoplankton in T1	−33.9	6.6
Soil organic matter		
Soil in a Castanopsis fargesii field	−21.0	13.3
Soil in a Loropetalum chinense field	−24.9	13.3
Soil in a *Pinus massoniana* field	−21.8	13.4
Soil in a *Pinus elliottii* field	−23.6	13.7
Soil in a Eucalypt field	−25.2	12.5
Soil in a Bamboo field	−22.4	13.0

to 12.20 and 2.52 to 15.72 mg/L in summer and winter, respectively. However, obvious spatial variations of NO_3^- concentrations ($p < 0.01$) were observed increasing significantly from the upper to the lower reaches in both seasons (Fig. 1), especially in summer. The DIC concentrations varied from 3.6 to 42.0 mg/L, with a mean value of 20.6 mg/L, and showed significant seasonal variations, with higher concentrations in winter and lower concentrations in summer ($p < 0.01$), which is possibly affected by both rainwater dilution and water–rock interactions (Zhao et al., 2020b). During summer, the dissolution of carbonate rocks is accelerated due to the high temperature, high humidity and strong hydrodynamic conditions. However, the abundant rainfall also causes strong dilution of DIC during summer. River discharge was higher during summer in comparison to winter in all stations. The increase was between 700% and 1000% higher in summer in most stations (Table S3). Compared with the several orders of magnitude variations of river discharge changes, the seasonal variations of rock weathering rate are insignificant. Therefore, the river discharge plays a dominant role in the variations of riverine ionic concentrations (Zhao et al., 2020b). Although the river discharge increased by 159% and 228% going downstream in summer and winter, respectively, and 78% and 130% of which were from tributaries, the DIC concentrations increased gradually from the upper reaches to the lower reaches. This variation is related to the spatial distribution of carbonate rocks in the Lijiang River basin (Fig. S1). The POC concentrations ranged from 0.09 to 0.75 mg/L (Table S4). On average, POC concentrations only accounted for 15% and 7% of OC in summer and winter, respectively, suggesting that DOC is the main constituent of OC in the Lijiang River. Although the DOC concentrations did not show different seasonal variations ($p > 0.05$), significant spatial variations ($p < 0.05$) of the DOC concentrations could be found, increasing significantly from the upper to the mid-lower reaches in the Lijiang River. The downstream increase in DOC concentrations may be related to the DIC fertilization (Yang et al., 2016). The higher DIC concentrations in the mid-lower reaches can promote the aquatic photosynthesis. The overall DON concentrations varied from 0.19 to 0.56 mg/L with a lower average in summer (0.31 ± 0.07 mg/L) than in winter (0.41 ± 0.10 mg/L), and spatially, the DON concentrations exhibited a similar variation to the DOC in the Lijiang River. The DOC/DON ratios in the Lijiang River ranged from 8.29 to 11.47 with a higher average value in summer (10.48 ± 0.59) than in winter (9.35 ± 0.78) and decreased in a fluctuating manner along the river in both seasons (Fig. 1).

The $\delta^{13}C_{DIC}$ values showed significant seasonal ($p < 0.01$) and spatial variations ($p < 0.01$) in the Lijiang River (Fig. 1). The $\delta^{13}C_{DIC}$ values in summer were obviously lighter than that in winter, ranging from −11.8‰ to −9.0‰ in summer and −10.3‰ to −7.2‰ in winter, respectively. The higher $\delta^{13}C_{DIC}$ values were observed in the middle reaches in summer, whereas in winter, the $\delta^{13}C_{DIC}$ values increased along the river. The $\delta^{13}C_{DOC}$ values varied from −29.6‰ to −23.4‰ with a higher average in summer (−25.8‰ ± 1.5‰) and a lower average in winter (−26.9‰ ± 1.7‰). Spatially, the $\delta^{13}C_{DOC}$ values in the Lijiang River generally decreased along the river with slight fluctuating at downstream in both seasons. The $\delta^{15}N\text{-}NO_3^-$ and $\delta^{18}O\text{-}NO_3^-$ values exhibited significantly seasonal variations ($p < 0.01$), showing higher values in winter and lower values in summer in the Lijiang River (Fig. 1). Also, the $\delta^{15}N\text{-}NO_3^-$ and $\delta^{18}O\text{-}NO_3^-$ values exhibited significant spatial variations ($p < 0.01$) in the Lijiang River (Fig. 1). The $\delta^{15}N\text{-}NO_3^-$ and $\delta^{18}O\text{-}NO_3^-$ values were higher in the middle reaches than that in the upper and lower reaches in summer, while in winter, these values increased along the river.

4.3. Diurnal variations in hydrochemistry and $\delta^{13}C_{DIC}$, $\delta^{15}N\text{-}NO_3^-$, and $\delta^{18}O\text{-}NO_3^-$ of the water at site M6 of the Lijiang River

As shown in Fig. 2, pronounced cyclic diel variations in hydrochemistry and isotopes of water were observed in the middle reaches (site M6) of the Lijiang River. Two significant differences of variational patterns with different amplitudes for the river water could be found on the diurnal timescale, of which water temperature, pH, DO, DOC, $\delta^{13}C_{DIC}$, $\delta^{15}N\text{-}NO_3^-$ and $\delta^{18}O\text{-}NO_3^-$ increased during the day and decreased at night, while pCO_2, DIC and NO_3^- had the opposite trend. Water temperature varied from 17.66 to 21.49 °C (mean = 19.62 °C) with the highest temperature occurring in the afternoon (15:00–16:00) and the lowest temperature at dawn (05:00–06:00). pH varied from 9.08 during the day to 7.06 at night, which was consistent with DO variations (5.77 mg/L at night to 25.17 mg/L at daytime). The maximum values corresponding to both of these parameters occurred in the early afternoon (14:00–16:00). The curves of pH and DO flattened in the evening and remained constant until the next morning. The peak values were maintained for 2–3 h. pCO_2, DIC and NO_3^- showed synchronous but opposite diel patterns with respect to pH and DO with their lowest values occurring in the afternoon and highest values at night and in the early morning (Fig. 2). The values of these parameters increased from low values in the evening to peak values at sunrise. The maxima of pCO_2, DIC and NO_3^-, viz. 2500–3000 ppmv, 20–23 mg/L and 8.82–9.21 mg/L, respectively, occurred at 04:00–06:00 while their respective minima of 47–98 ppmv, 14–15 mg/L and 6.34–6.89 mg/L occurred at around 14:00–16:00. The mean DOC concentration was 3.63 mg/L with a diel range of 3.26 (just prior to sunrise) to 3.98 (in the afternoon) mg/L.

The $\delta^{13}C_{DIC}$ values showed diel variations with a minimum of −9.4‰ at 04:00–06:00 and a maximum of −8.1‰ at 14:00–16:00 (Fig. 2). The $\delta^{13}C_{DIC}$ maxima corresponded to NO_3^-, DIC and pCO_2 minima, while the $\delta^{13}C_{DIC}$ minima corresponded to pH, DO, water temperature and DOC minima. The $\delta^{15}N\text{-}NO_3^-$ values varied from 3.8‰ to 5.7‰ with a mean of 4.7‰ and $\delta^{18}O\text{-}NO_3^-$ values varied from 6.1‰ to 8.4‰ with a mean of 7.2‰. Meanwhile, both $\delta^{15}N\text{-}NO_3^-$ and $\delta^{18}O\text{-}NO_3^-$ values displayed minima values at nighttime and maxima values at afternoon during a day.

5. Discussion

5.1. Source apportionment of DOC in the karst aquatic system of the Lijiang River

As shown in Fig. 3, the proportional contributions of DOC from three potential sources exhibited seasonal and spatial variations in the Lijiang

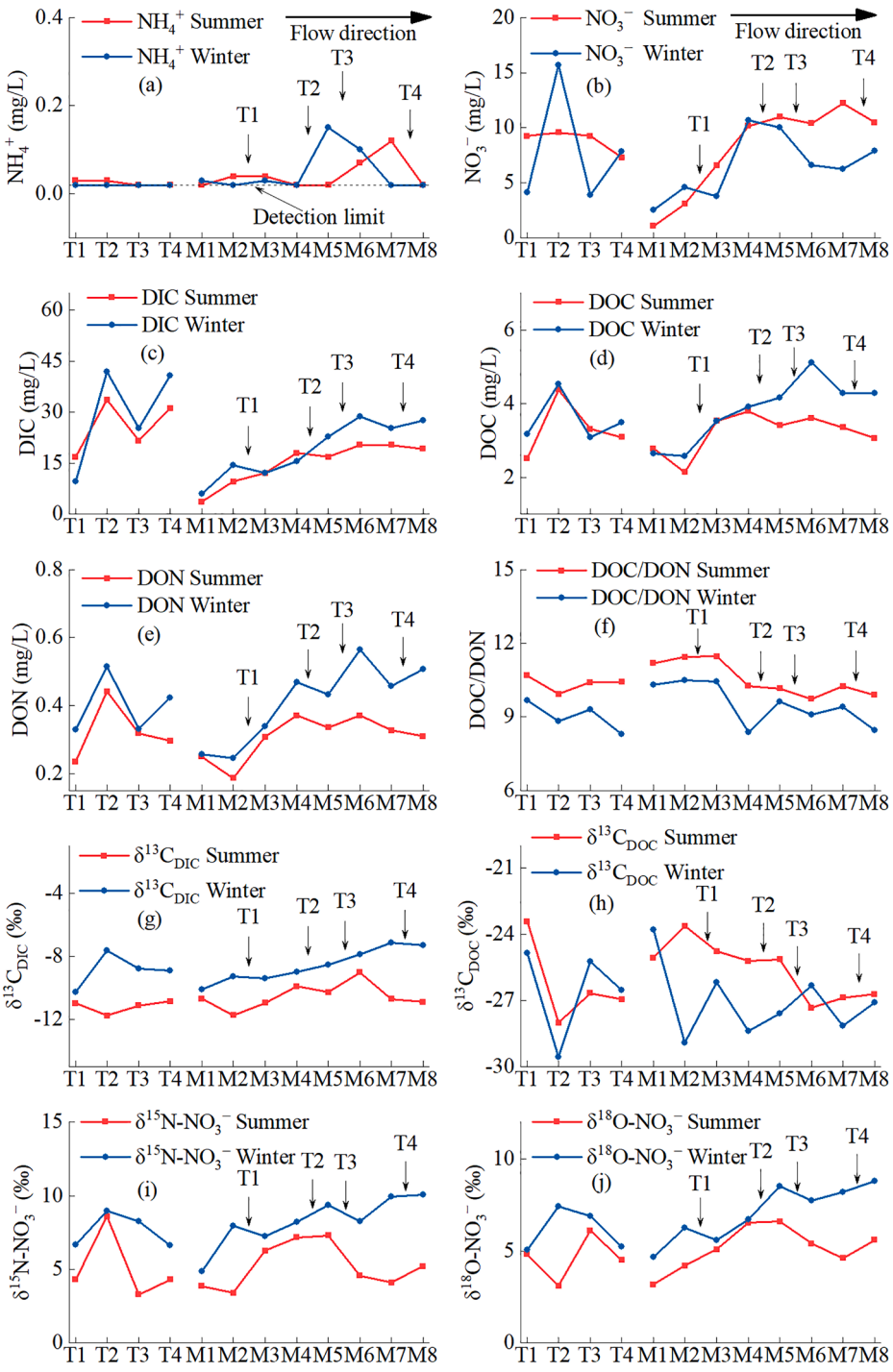

Fig. 1. Variations in NH_4^+, NO_3^-, DIC, DOC and DON concentrations, DOC/DON, $\delta^{13}C_{DIC}$, $\delta^{13}C_{DOC}$, $\delta^{15}N\text{-}NO_3^-$, and $\delta^{18}O\text{-}NO_3^-$ values in the Lijiang River in summer and winter.

River. In summer, DOC of the water in the Lijiang River was primarily derived from the soil organic matter (about 50%), and then from phytoplankton (around 27%) and macrophytes (around 23%). In winter, DOC of the water in the Lijiang River was primarily derived from the phytoplankton (about 37%) and macrophytes (around 35%), and then from soil organic matter (about 28%). These results indicate that autochthonous organic sources act as the dominant inputs in both seasons in the Lijiang River (Fig. 3). This is similar to the result of Waterson and Canuel (2008), their study showed that the contribution of autochthonous OC was about 62% in the Mississippi River.

Soil organic matter input increased by ~12% in summer compared with that in winter, which might be attributed to more flushing of soil organic matter from hill slopes to rivers under the intense rainfall conditions (Li et al., 2019). The contributions of phytoplankton and macrophytes sources were approximately 10% higher in winter than that in summer. Moreover, the DOC/DON ratios in the Lijiang River were higher in summer than that in winter, suggesting that the ratios of autochthonous/allochthonous DOC were different in both seasons due to higher C/N ratios of terrestrial plants and lower C/N ratios of phytoplankton. In winter, the riverine primary production plays an important role because of longer residence time and improved light intensity for river water under lower flow discharge, both of which favor

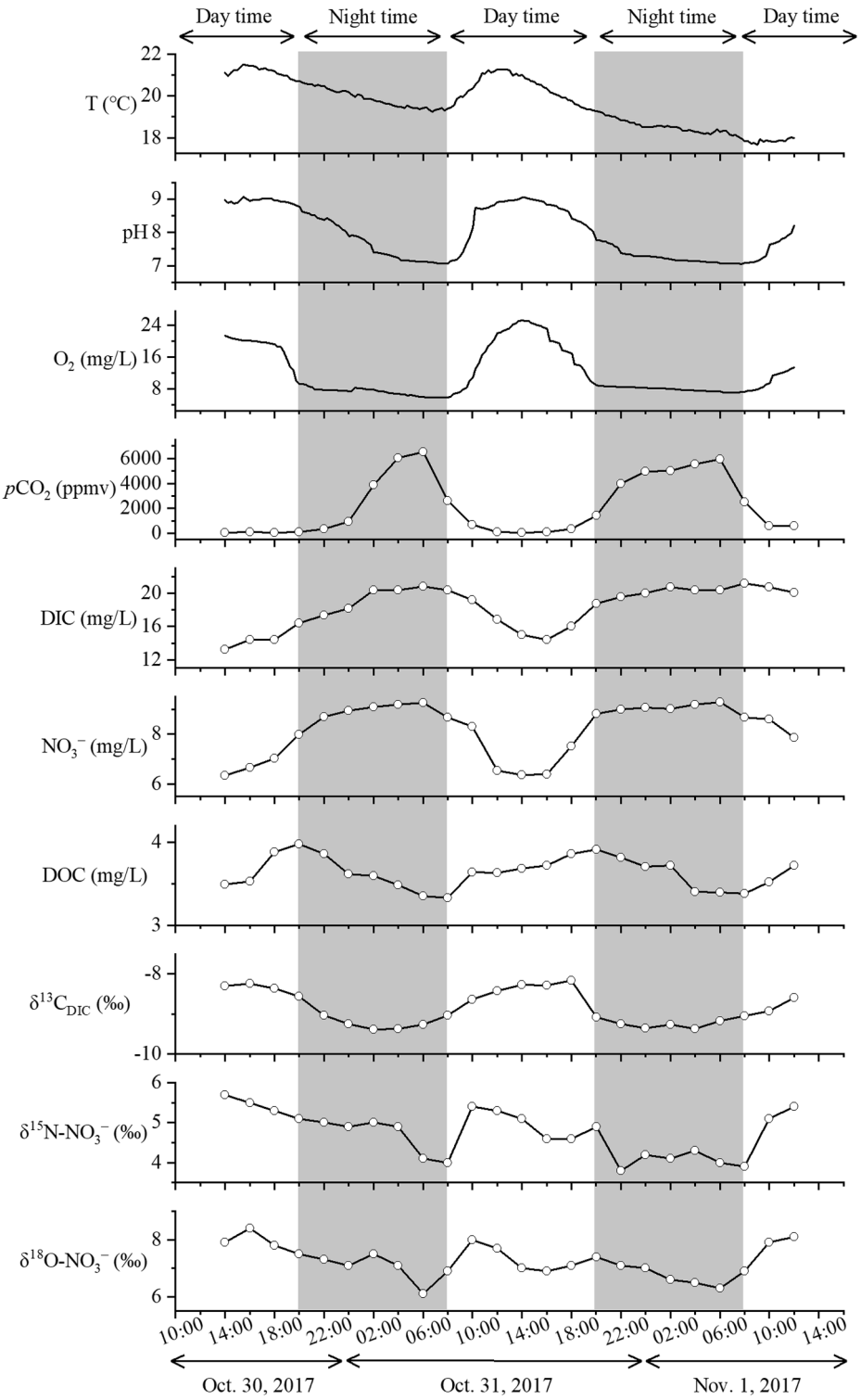

Fig. 2. Diurnal changes in hydrochemistry, $\delta^{13}C_{DIC}$, $\delta^{15}N\text{-}NO_3^-$, and $\delta^{18}O\text{-}NO_3^-$ of the water at site M6 of the Lijiang River over three days from October 30 to November 1, 2017.

aquatic photosynthesis (Cao et al., 2003; Sun et al., 2015). In summer, the aquatic photosynthesis is restricted by shorter residence time, weaker incident light and higher turbidity of river water (Huang et al., 2004; Sun et al., 2015). Insignificant differences in the contribution of macrophytes between the upper and the mid-lower reaches in both seasons suggest that the DOC derived from macrophytes is a stable autochthonous source of DOC for the water along the Lijiang River. Meanwhile, the contribution of phytoplankton in the mid-lower reaches was higher than that in the upper reaches in both seasons, suggesting that the DOC derived from phytoplankton is an increasing autochthonous source of DOC for the water along the Lijiang River. The contribution of soil organic matter showed an opposite spatial change to that of the phytoplankton. The DOC/DON ratios of the water in the Lijiang River showed a downstream decreasing trend in both seasons, which also indicates a downstream increase of autochthonous fraction in the riverine DOC (Sun et al., 2015). Higher autochthonous DOC

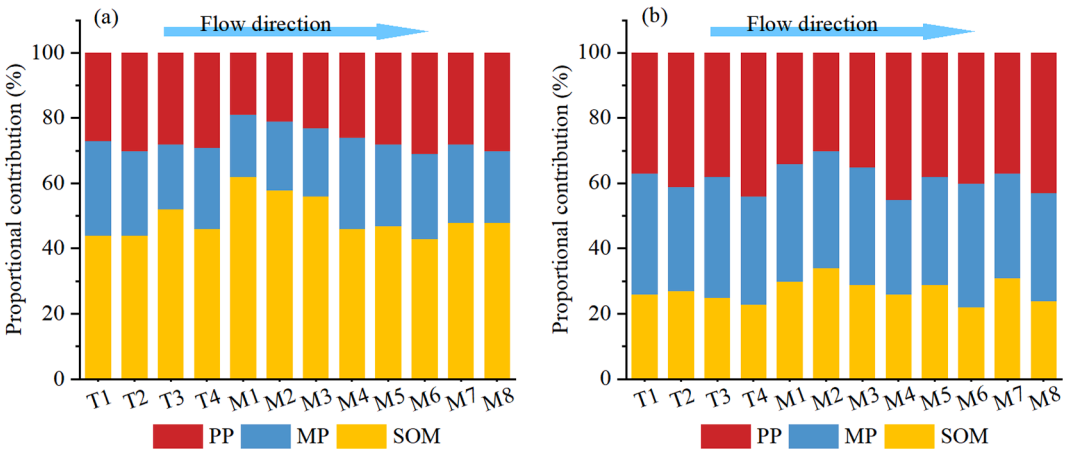

Fig. 3. Seasonal and spatial variations in the proportional contributions (mean probability estimate) of different DOC sources in the Lijiang River estimated by SIAR. (a) Summer and (b) winter.

contribution derived from phytoplankton and lower contribution from soil organic matter in the mid-lower reaches related to the high concentrations of DIC and NO_3^- and slow river flow in the mid-lower reaches, suggesting that higher DIC and NO_3^- concentrations could promote the growth of phytoplankton in karst aquatic systems (Wang et al., 2018; Yang et al., 2016; Zeng et al., 2019), and a condition of slow flow is also favorable for in-situ phytoplankton production (Sun et al., 2015).

According to Eq. (3), the autochthonous DOC concentrations derived from phytoplankton and macrophytes varied from 1.09 to 2.43 and 1.70 to 3.44 mg/L in summer and winter, respectively. As shown in Fig. 4, there were positive correlations between autochthonous DOC and DIC, NO_3^-, $\delta^{13}C_{DIC}$, and $\delta^{15}N\text{-}NO_3^-$ in both seasons (Fig. 4), indicating that DIC and NO_3^- variations could be closely related to the formation of autochthonous DOC in the Lijiang River. This is supported by the positive correlation of DIC and NO_3^- (Fig. 5). Moreover, it is worth noting that these correlations were consistently weaker in summer due to weaker aquatic photosynthesis. Thus, we could conclude that the transformation of DIC and NO_3^- and the formation of autochthonous DOC are coupled in the karst aquatic system of the Lijiang River. However, high-resolution monitoring is required for a better understanding of the coupled DIC and NO_3^- cycling and the formation of autochthonous DOC.

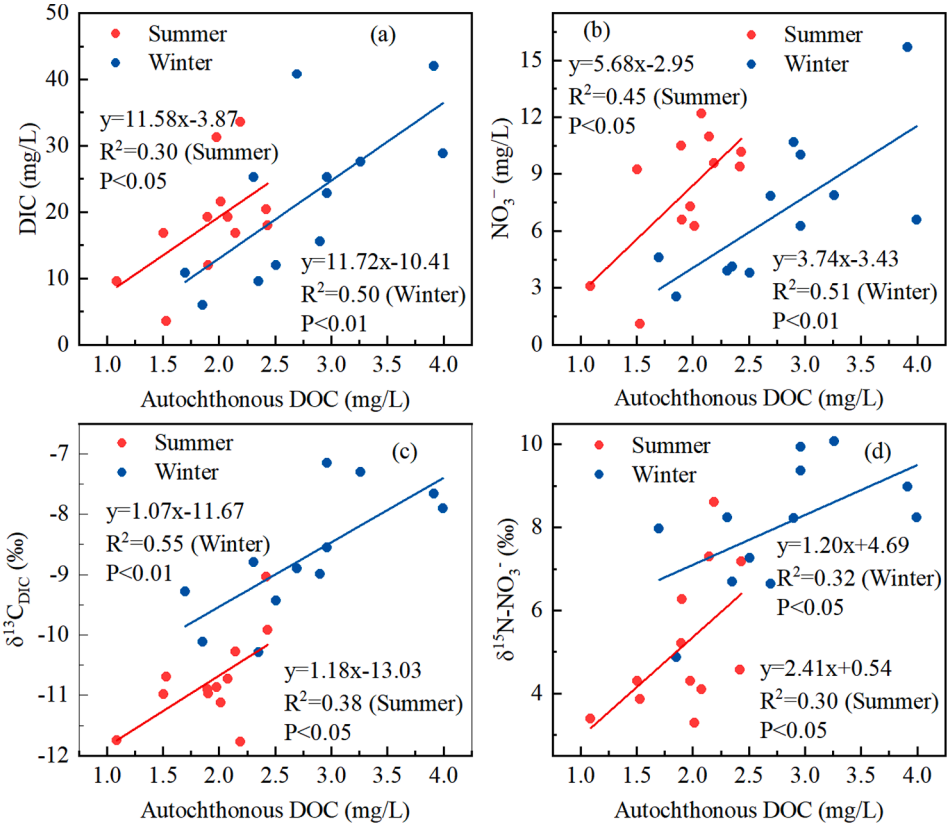

Fig. 4. Relationships between autochthonous DOC and (a) DIC, (b) NO_3^-, (c) $\delta^{13}C_{DIC}$, and (d) $\delta^{15}N\text{-}NO_3^-$ in the Lijiang River.

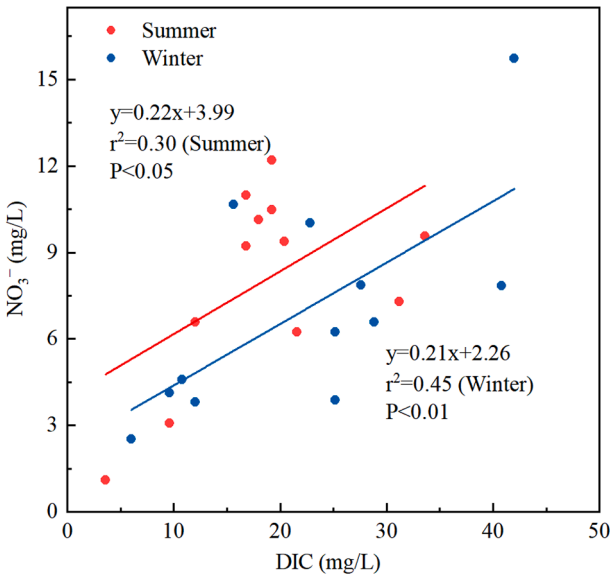

Fig. 5. Relationship between DIC and NO_3^- in the Lijiang River.

5.2. Coupled DIC and NO_3^- cycling controls the formation of autochthonous DOC in the karst aquatic system of the Lijiang River

5.2.1. Evidence from hydrogeochemistry

As shown in Table 2, as expected, there was an apparent positive relationship ($R^2 = 0.48$) between water temperature and DO (Table 2) and DO exhibited an inverse relationship with pCO_2 ($R^2 = 0.52$) and DIC ($R^2 = 0.81$) over a given diel cycle at site M6 of the Lijiang River. However, there was a positive correlation between DOC and DO of the river water during the diurnal monitoring period. These suggest that in-stream metabolism rather than air temperature and degassing controls the daily variations of DIC concentrations. Heffernan and Cohen (2010) and Cohen et al. (2012) have found that denitrification can decrease NO_3^- concentrations due to the consumption of O_2 and the production of CO_2 at night. However, the increased NO_3^- concentrations at night and negative correlation between NO_3^- and DO ($R^2 = 0.41$) (Table 2) suggest that the denitrification is not the main factor controlling the concentrations of NO_3^- in the Lijiang River.

As shown in Table 2, DIC and NO_3^- were negatively correlated with DOC and DO, respectively, but exhibited positive correlations with pCO_2, indicating that the diurnal variations in DIC, NO_3^- and DOC can be attributed primarily to the metabolic activities of subaquatic communities in the Lijiang River. According to the calculation, the total DIC loss due to subaquatic communities during the diurnal period was estimated to be ~320,165 mol (accounting for 70% of the total DIC loss), implying that the DIC consumption by subaquatic communities was 160,082 mol/day (Fig. 6). The total NO_3^- consumption due to the metabolism of

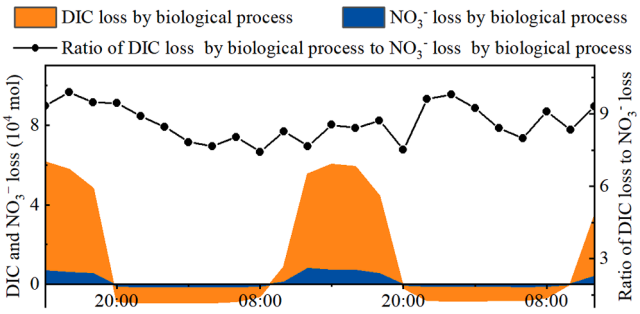

Fig. 6. Calculated DIC and NO_3^- consumption due to metabolism of subaquatic communities and the ratio of consumed DIC to consumed NO_3^- at site M6 in a 48-h timescale from 14:00 on October 30 to 12:00 on November 1. Positive values represent DIC and NO_3^- consumption by photosynthesis while negative values represent DIC and NO_3^- gain by respiration.

subaquatic communities during the monitoring period was ~36,276 mol (i.e. 18,138 mol/day) (Fig. 6). Furthermore, during photosynthesis, DIC and NO_3^- were consumed in the ratio of ~9:1 (mol/mol) (Fig. 6), which lies between the C/N ratios of aquatic plants (mean = 11) and phytoplankton (mean = 6.4). This ratio fits well with the DOC/DON ratios of the water in the Lijiang River, ranging from 8.29 to 11.47.

As shown in Fig. 7, DIC and NO_3^- will be consumed by the metabolism of subaquatic communities, resulting in an increase in DOC concentrations in the river water, if NEP is positive (GPP > ER). DIC and NO_3^- will be produced if NEP is negative (GPP < ER), resulting in a decline in DOC concentrations in the river water. During the diurnal monitoring period, assimilation was estimated to be 6.2% and 7.1% of the total DIC and NO_3^- flux, respectively. The proportions of DIC and NO_3^- utilized on the diurnal scale were comparable with the values estimated on the interannual scale (assimilation of DIC and NO_3^- were estimated to be 6.1% and 7.4% of the total DIC and NO_3^- flux, respectively). However, there were seasonal differences in the proportions of DIC and NO_3^- utilized in the Lijiang River, which are higher in the dry season (7.3% and 7.9% of the total DIC and NO_3^- flux, respectively) than those in the wet season (5.2% and 6.4% of the total DIC and NO_3^- flux, respectively). This is resulted from different residence time, turbidity and light of river water in both seasons. The longer residence time, lower turbidity and improved light for river water in winter could promote the aquatic photosynthesis (Cao et al., 2003; Sun et al., 2015), while the shorter residence time, higher turbidity and weaker light caused by high precipitation in summer could restrict the aquatic photosynthesis (Huang et al., 2004; Sun et al., 2015).

5.2.2. Evidence from isotopes

$\delta^{13}C_{DIC}$ can be affected by the combined effects of gas exchange with the atmosphere, metabolism of subaquatic communities and carbonate mineral dissolution and precipitation in karst aquatic systems (de Montety et al., 2011; Jiang et al., 2013). Such processes controlling DIC

Table 2
Correlation coefficients between selected physico-chemical parameters at site M6 of the Lijiang River during the diurnal monitoring period.

	T	pH	DO	pCO_2	DIC	NO_3^-	DOC	$\delta^{13}C_{DIC}$	$\delta^{15}N\text{-}NO_3^-$	$\delta^{18}O\text{-}NO_3^-$
T	1	0.81**	0.69**	−0.58**	−0.84**	−0.79**	0.42*	0.68**	0.62**	0.49*
pH		1	0.92**	−0.85**	−0.92**	−0.70**	0.64**	0.93**	0.81**	0.61**
DO			1	−0.72**	−0.90**	−0.64**	0.76**	0.91**	0.74**	0.53*
pCO_2				1	0.72**	0.64**	−0.61**	−0.86**	−0.68**	−0.71**
DIC					1	0.88**	−0.56**	−0.84**	−0.73**	−0.59*
NO_3^-						1	−0.62**	−0.76**	−0.72**	−0.61**
DOC							1	0.73**	0.48*	0.38*
$\delta^{13}C_{DIC}$								1	0.76**	0.60**
$\delta^{15}N\text{-}NO_3^-$									1	0.84**
$\delta^{18}O\text{-}NO_3^-$										1

** Correlation is significant at the 0.01 level.
* Correlation is significant at the 0.05 level.

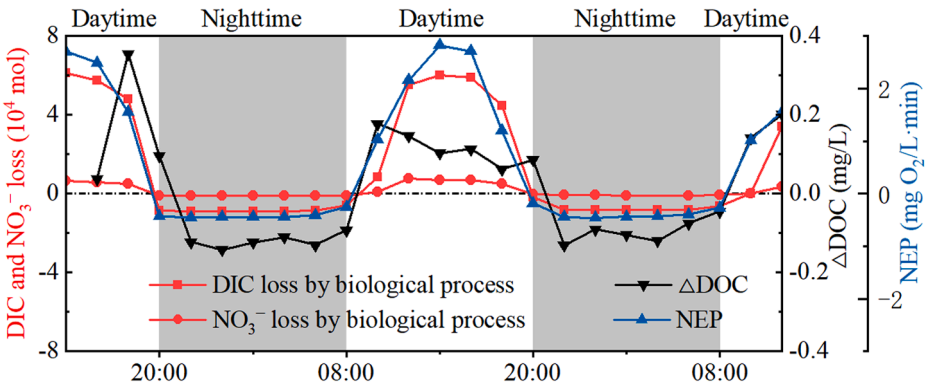

Fig. 7. DIC and NO_3^- loss due to metabolism of subaquatic communities and changes in DOC at M6 in a 48-h timescale from 14:00 on October 30 to 12:00 on November 1 ($\triangle DOC = DOC_{(t)} - DOC_{(t-1)}$). Positive values represent DIC and NO_3^- loss by photosynthesis while negative values represent DIC and NO_3^- gain by respiration. Positive NEP indicate GPP > ER and negative NEP indicate GPP < ER.

cycling may thus be reflected in diel variations in the $\delta^{13}C_{DIC}$ of river water (de Montety et al., 2011). The isotopic compositions of NO_3^- are governed by isotopic fractionation during biogeochemical processes, such as assimilation, nitrification and denitrification. The nitrification is a multi-step process of oxidizing organic nitrogen to NO_3^- (Xu et al., 2016). In theory, $\delta^{18}O$ values of NO_3^- produced by microbial nitrification would have approximately one-third of the oxygen derived from oxygen in the air ($\delta^{18}O$-O_2), while two-thirds should be derived from ambient water oxygen ($\delta^{18}O$-H_2O) (Andersson and Hooper, 1983). The $\delta^{18}O$ value of oxygen in the air is about 23.9‰ (Barkan and Luz, 2005), and the $\delta^{18}O$-H_2O values ranged from −5.6‰ to −5.0‰ (Fig. S4) in the Lijiang River. Therefore, the calculated $\delta^{18}O$-NO_3^- values produced from the nitrification ranged from 4.3‰ to 4.7‰ in the water of the Lijiang River. However, as stated in previous section, the $\delta^{18}O$-NO_3^- values varied from 6.1‰ to 8.4‰ in the water of the Lijiang River, which were higher than the theoretical $\delta^{18}O$-NO_3^- values. These shifts of the measured values from the calculated $\delta^{18}O$-NO_3^- values in the water of Lijiang River, could be resulted from other biological processes (Mayer et al., 2001). $\delta^{13}C_{DIC}$, $\delta^{15}N$-NO_3^- and $\delta^{18}O$-NO_3^- were positively correlated with DO and DOC, and negatively correlated with DIC and NO_3^-, respectively (Table 2). Moreover, in isotopic coupling, the slope of $\delta^{15}N$-NO_3^- and $\delta^{18}O$-NO_3^- curve was calculated to be 0.98 (Fig. S5). The linear relationship between $\delta^{15}N$-NO_3^- and $\delta^{18}O$-NO_3^- (1.3:1 to 2.1:1) can also provide an evidence for the denitrification (Lee et al., 2008; Xue et al., 2009); i.e., the slope of $\delta^{18}O$-NO_3^- relative to $\delta^{15}N$-NO_3^- ranges from 0.48 to 0.76. However, the slope of the line relating $\delta^{15}N$-NO_3^- and $\delta^{18}O$-NO_3^- was not in this range while the DO concentrations ranged from 5.77 to 25.17 mg/L. As revealed by some studies, the removal of NO_3^- via the denitrification is insignificant for well oxygenated rivers (Ribot et al., 2017; Soto et al., 2018). These results suggest that the denitrification is insignificant in the Lijiang River. Meanwhile, the amounts of NO_3^- produced and DOC consumed by the nitrification process could be very small, because the values of $\delta^{15}N$-NO_3^- and $\delta^{18}O$-NO_3^- were dominantly affected by the aquatic photosynthesis. Thus, we can also conclude that the metabolism of subaquatic communities controls the DIC and NO_3^- transformations in the Lijiang River as well as the DOC concentrations.

As shown in Fig. 8, the $\delta^{13}C_{DIC}$ was enriched by 7.9‰ (3.9‰/day) during photosynthesis and depleted by −2.2‰ (−1.1‰/day) during respiration, of which 4.0‰ and 3.9‰ of $\delta^{13}C_{DIC}$ were enriched by phytoplankton and macrophytes, respectively, while −1.2‰ and −1.0‰ of $\delta^{13}C_{DIC}$ were depleted by phytoplankton and macrophytes, respectively. Calcite carbonate precipitation and dissolution and CO_2 outgassing showed negligible effects on the $\delta^{13}C_{DIC}$ transformation. The $\delta^{15}N$-NO_3^- and $\delta^{18}O$-NO_3^- were enriched by 10.6‰ (5.3‰/day) and 11.2‰ (5.6‰/day) during photosynthesis and depleted by −0.8‰ (−0.4‰/day) and −0.9‰ (−0.5‰/day) during respiration, respectively. These results confirmed that the DIC and NO_3^- transformations in the water of the Lijiang River were primarily controlled by the metabolism of subaquatic communities.

5.3. *Contributions of the coupled C—N cycling to the C and N sinks in the karst aquatic system of the Lijiang River*

Our results demonstrate that the coupled C—N cycling involving DIC and NO_3^- leads to the variations in DOC concentrations via the metabolism of subaquatic communities in the Lijiang River. Annually, about 1.18×10^7 kg C/yr of DIC (Eq. (4)) and 1.64×10^6 kg N/yr of NO_3^- (Eq. (5)) were converted into organic matter by the aquatic photosynthesis in the Lijiang River, with 80% and 79% of the DIC and NO_3^- consumption produced in the wet season, respectively. The higher DIC and NO_3^- concentrations in karst aquatic systems could fuel the growth of subaquatic communities, which in turn could enhance the uptake of DIC and NO_3^- and result in the DOC accumulation in the river water. This implies that the coupling cycle of DIC and NO_3^- can promote the

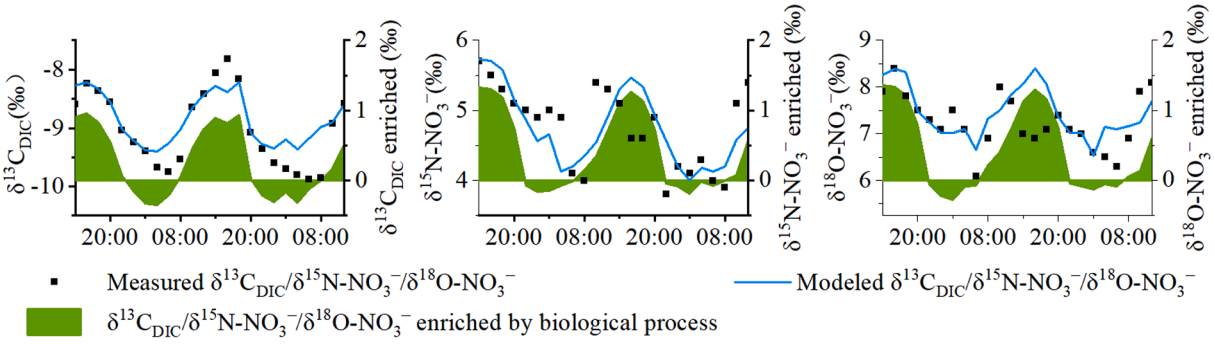

Fig. 8. The measured and modeled values of $\delta^{13}C_{DIC}/\delta^{15}N$-$NO_3^-/\delta^{18}O$-$NO_3^-$ and $^{13}C/^{15}N/^{18}O$ fractionation enrichment due to biological process.

formation of autochthonous DOC and thus produce significant net C and N sinks in karst aquatic systems.

6. Conclusions

In this study, seasonal and diurnal monitoring data of DIC, DOC and NO_3^- concentrations, $\delta^{13}C_{DIC}$, $\delta^{13}C_{DOC}$, $\delta^{15}N\text{-}NO_3^-$, and $\delta^{18}O\text{-}NO_3^-$, and other hydrochemical parameters of the water were used to quantify the consumption of DIC and NO_3^- and the DOC formation in the coupled C—N cycling in the Lijiang River, a typical karst aquatic system in Southwest China. The results of the SIAR model indicated that ~50% and 72% of the total DOC formed in summer and winter, respectively, corresponded to autochthonous OC (formed in the coupled C—N cycling). In addition, the contribution of autochthonous OC in the mid-lower reaches was higher than that in the upper reaches. The results of diurnal monitoring indicated that the DIC and NO_3^- transformations in the water of the Lijiang River were mainly controlled by the metabolic processes (photosynthesis and respiration) of subaquatic communities, accompanied by DOC generation. The DIC and NO_3^- were consumed during aquatic photosynthesis in the ratio of 9:1 (mol/mol) to produce autochthonous DOC. At the same time, $\delta^{13}C_{DIC}$, $\delta^{15}N\text{-}NO_3^-$ and $\delta^{18}O\text{-}NO_3^-$ were enriched by 7.9‰, 10.6‰ and 11.2‰ daily, respectively, during the aquatic photosynthesis. On the diurnal scale, 6.2% of the total DIC and 7.1% of the total NO_3^- were consumed by metabolic processes. These values were comparable with the corresponding values on the interannual scale of the Lijiang River. However, the proportions of DIC and NO_3^- utilized in the dry season were higher than those in the wet season. 1.18×10^7 kg C/yr of DIC and 1.64×10^6 kg N/yr of NO_3^- were converted by the aquatic photosynthesis into organic matter in the coupled C—N cycling, most of the DIC and NO_3^- consumption produced in the wet season. Finally, our study illustrates that the coupled C—N cycling involving DIC and NO_3^- promotes the formation of autochthonous DOC and produces significant net C and N sinks in karst aquatic systems.

CRediT authorship contribution statement

Haijuan Zhao: Conceptualization, Investigation, Data curation, Methodology, Formal analysis, Writing - original draft, Writing - review & editing. **Yongjun Jiang:** Conceptualization, Investigation, Data curation, Project administration, Resources, Writing - original draft, Writing -review & editing, Funding acquisition, Supervision. **Qiong Xiao:** Conceptualization, Investigation, Methodology, Data curation, Writing - original draft, Funding acquisition. **Cheng Zhang:** Conceptualization, Methodology, Data curation, Writing - original draft, Funding acquisition. **Hamid M. Behzad:** Conceptualization, Resources, Writing - review & editing.

Declaration of competing interest

The authors declare that they have no known competing financial interests or personal relationships that could have appeared to influence the work reported in this paper.

Acknowledgement

This research was supported by the National Key Research and Development Program of China (2016YFC0502306), National Natural Science Foundation of China (41472321), the Basic Scientific Research of Chinese Academy of Geological Sciences (JYYWF20182002), the Special Fund for Basic Scientific Research of Chinese Academy of Geological Sciences (YYWF201639), the Guangxi Natural Science Foundation (2016GXNSFAA380064 and 2018GXNSFDA050002), the Graduate Scientific Research and Innovation Foundation of Chongqing (CYB19073), Chongqing Municipal Science and Technology Commission Fellowship Fund (CSTC2017jcyj-ysxX0004, CSTC2018jcyj-yszx0013), and International Partnership Program of Chinese Academy of Sciences (132852KYSB20170029-01). Special thanks are given to Zhijun Wang for his help with language editing and to Qigang Wang, Ying Miao, and Yongli Guo for their help with field and laboratory work.

Appendix A. Supplementary data

Supplementary data to this article can be found online at https://doi.org/10.1016/j.jhydrol.2020.125764.

References

Andersson, K.K., Hooper, A.B., 1983. O_2 and H_2O are each the source of one O in NO_2^- produced from NH_3 by Nitrosomonas: ^{15}N-NMR evidence. Fed. Eur. Biochem. Soc. 164, 236–240. https://doi.org/10.1016/0014-5793(83)80292-0.

Barkan, E., Luz, B., 2005. High precision measurements of $^{17}O/^{16}O$ and $^{18}O/^{16}O$ ratios in H_2O. Rapid Commun. Mass Spectrom. 19, 3737–3742. https://doi.org/10.1002/rcm.2250.

Beusen, A., Bouwman, A., Beek, L., Mogollón, J., Middelburg, J., 2015. Global riverine N and P transport to ocean increased during the twentieth century despite increased retention along the aquatic continuum. Biogeosci. Discuss. 12, 20123–20148. https://doi.org/10.5194/bgd-12-20123-2015.

Cao, J., Lee, S., Ho, K.F., Zou, S., Zhang, X., Pan, J., 2003. Spatial and seasonal distributions of atmospheric carbonaceous aerosols in Pearl River Delta region, China. China Particuology 1, 33–37. https://doi.org/10.1016/S1672-2515(07)60097-9.

Cohen, M., Heffernan, J., Albertin, A., Martin, J., Cohen, C., Heffernan, J., Albertin, A., Martin, J., 2012. Inference of riverine nitrogen processing from longitudinal and diel variation in dual nitrate isotopes. J. Geophys. Res. 117, G0121. https://doi.org/10.1029/2011JG001715.

de Montety, V., Martin, J.B., Cohen, M.J., Foster, C., Kurz, M.J., 2011. Influence of diel biogeochemical cycles on carbonate equilibrium in a karst river. Chem. Geol. 283, 31–43. https://doi.org/10.1016/j.chemgeo.2010.12.025.

del Giorgio, P.A., Williams, P.J., 2015. Respiration in wetland ecosystems. Oxford University Press, New York. https://doi.org/10.1093/acprof.

Demars, B., Thompson, J., Manson, J., 2015. Stream metabolism and the open diel oxygen method: principles, practice, and perspectives: problems in stream metabolism studies. Limnol. Oceanogr. Methods 13, 356–374. https://doi.org/10.1002/lom3.10030.

Goñi, M.A., Teixeira, M.J., Perkey, D.W., 2003. Sources and distribution of organic matter in a river-dominated estuary (Winyah Bay, SC, USA). Estuar. Coast. Shelf Sci. 57, 1023–1048. https://doi.org/10.1016/S0272-7714(03)00008-8.

Granger, J., Sigman, D., Needoba, J., Harrison, P., 2004. Coupled nitrogen and oxygen isotope fractionation of nitrate during assimilation by cultures of marine phytoplankton. Limnol. Oceanogr. 49, 1763–1773. https://doi.org/10.4319/lo.2004.49.5.1763.

Gruber, N., Galloway, J., 2008. An earth-system perspective of the global nitrogen cycle. Nature 451, 293–296. https://doi.org/10.1038/nature06592.

Hamilton, S.K., Sippel, S.I., Bunn, S.E., 2005. Separation of algae from detritus for stable isotope or ecological stoichiometry studies using density fractionation in colloidal silica. Limnol. Oceanogr. Methods 3, 149–157. https://doi.org/10.4319/lom.2005.3.149.

Heffernan, J., Cohen, M., 2010. Direct and indirect coupling of primary production and diel nitrate dynamics in a subtropical spring-fed river. Limnol. Oceanogr. 55, 677–688. https://doi.org/10.4319/lo.2009.55.2.0677.

Huang, L., Jian, W., Song, X., Huang, X., Liu, S., Qian, P.-Y., Yin, K.D., Wu, M., 2004. Species diversity and distribution for phytoplankton of the Pearl River estuary during rainy and dry seasons. Mar. Pollut. Bull. 49, 588–596. https://doi.org/10.1016/j.marpolbul.2004.03.015.

Jiang, Y., 2013. The contribution of human activities to dissolved inorganic carbon fluxes in a karst underground river system: evidence from major elements and $\delta^{13}C_{DIC}$ in Nandong, Southwest China. J. Contam. Hydrol. 152, 1–11. https://doi.org/10.1016/j.jconhyd.2013.05.010.

Jiang, Y., Hu, Y., Schirmer, M., 2013. Biogeochemical controls on daily cycling of hydrochemistry and $\delta^{13}C$ of dissolved inorganic carbon in a karst spring-fed pool. J. Hydrol. 478, 157–168. https://doi.org/10.1016/j.jhydrol.2012.12.001.

Jiang, Y., Lei, J., Hu, L., Xiao, Q., Wang, J., Zhang, C., Ali, H., 2020. Biogeochemical and physical controls on the evolution of dissolved inorganic carbon (DIC) and $\delta^{13}C_{DIC}$ in karst spring-waters exposed to atmospheric CO_2(g): insights from laboratory experiments. J. Hydrol. 583, 124294. https://doi.org/10.1016/j.jhydrol.2019.124294.

Kendall, C., Silva, S.R., Kelly, V.J., 2001. Carbon and nitrogen isotopic compositions of particulate organic matter in four large river systems across the United States. Hydrol. Process. 15, 1301–1346. https://doi.org/10.1002/hyp.216.

Kendall, C., Elliott, E.M., Wankel, S.D., 2008. Tracing anthropogenic inputs of nitrogen to ecosystems. In: Stable Isotopes in Ecology and Environmental Science, Second edition, pp. 375–449. https://doi.org/10.1002/9780470691854.ch12.

Lee, K.S., Bong, Y.S., Lee, D., Kim, Y., Kim, K., 2008. Tracing the sources of nitrate in the Han River watershed in Korea, using $\delta^{15}N\text{-}NO_3^-$ and $\delta^{18}O\text{-}NO_3^-$ values. Sci. Total Environ. 395, 117–124. https://doi.org/10.1016/J.SCITOTENV.2008.01.058.

Li, C., Li, S.L., Yue, F.J., Liu, J., Zhong, J., Yan, Z.F., Zhang, R.C., Wang, Z.J., Xu, S., 2019. Identification of sources and transformations of nitrate in the Xijiang River using

nitrate isotopes and Bayesian model. Sci. Total Environ. 646, 801–810. https://doi.org/10.1016/j.scitotenv.2018.07.345.
Liu, Z., Macpherson, G.L., Groves, C., Martin, J.B., Yuan, D., Zeng, S., 2018. Large and active CO_2 uptake by coupled carbonate weathering. Earth-Science Rev. 182, 42–49. https://doi.org/10.1016/j.earscirev.2018.05.007.
Marcarelli, A., Kirk, R., Baxter, C., 2010. Predicting effects of hydrologic alteration and climate change on ecosystem metabolism in a western U.S. river. Ecol. Appl. 20, 2081–2088. https://doi.org/10.1890/09-2364.1.
Mariotti, A., Germon, J., Hubert, P., Kaiser, P., Letolle, R., Tardieux, A., Tardieux, P., 1981. Experimental determination of nitrogen kinetic isotope fractionation: some principles; illustration for the denitrification and nitrification processes. Plant Soil 62, 413–430. https://doi.org/10.1007/BF02374138.
Mayer, B., Bollwerk, S.M., Mansfeldt, T., Hütter, B., Veizer, J., 2001. The oxygen isotope composition of nitrate generated by nitrification in acid forest floors. Geochim. Cosmochim. Acta 65, 2743–2756. https://doi.org/10.1016/S0016-7037(01)00612-3.
Melnikov, N., O'Neill, B., 2006. Learning about the carbon cycle from global budget data. Geophys. Res. Lett. 33, L02075 https://doi.org/10.1029/2005GL023935.
Mook, W.G., 2006. Introduction to isotope hydrology. In: International Association of Hydrogeologists, International Contributions to Hydrogeology 25. Taylor and Francis/Balkema, London, 226 pp.
Nõges, P., Cremona, F., Laas, A., Martma, T., Rõõm, E.-I., Toming, K., Viik, M., Vilbaste, S., Nõges, T., 2016. Role of a productive lake in carbon sequestration within a calcareous catchment. Sci. Total Environ. 550, 225–230. https://doi.org/10.1016/j.scitotenv.2016.01.088.
Odum, H.T., 1956. Primary production in flowing waters. Limnol. Oceanogr. 1, 102–117.
Parnell, A.C., Inger, R., Bearhop, S., Jackson, A.L., 2010. Source partitioning using stable isotopes: coping with too much variation. PLoS One 5, 1–5. https://doi.org/10.1371/journal.pone.0009672.
Pedersen, O., Colmer, T., Sand-Jensen, K., 2013. Underwater photosynthesis of submerged plants – recent advances and methods. Front. Plant Sci. 4, 140. https://doi.org/10.3389/fpls.2013.00140.
Peterson, B.J., Wollheim, W.M., Mulholland, P.J., Webster, J.R., Meyer, J.L., Tank, J.L., Martí, E., Bowden, W.B., Valett, H.M., Hershey, A.E., McDowell, W.H., Dodds, W.K., Hamilton, S.K., Gregory, S., Morrall, D.D., 2001. Control of nitrogen export from watersheds by headwater streams. Science. 292, 86–90. https://doi.org/10.1126/science.1056874.
Pu, J., Li, J., Khadka, M., Martin, J., Zhang, T., Yu, S., Yuan, D., 2016. In-stream metabolism and atmospheric carbon sequestration in a groundwater-fed karst stream. Sci. Total Environ. 579, 1343–1355. https://doi.org/10.1016/j.scitotenv.2016.11.132.
Raymond, P.A., Oh, N.H., Turner, R.E., Broussard, W., 2008. Anthropogenically enhanced fluxes of water and carbon from the Mississippi River. Nature. 451, 449–452. https://doi.org/10.1038/nature06505.
Raymond, P., Zappa, C., Butman, D., Bott, T., Potter, J., Mulholland, P., Laursen, A., McDowell, W., Newbold, D., 2012. Scaling the gas transfer velocity and hydraulic geometry in streams and small rivers. Limnol. Oceanogr. Fluids Environ. 2, 41–53. https://doi.org/10.1215/21573689-1597669.
Ribot, M., Von Schiller, D., Martí, E., 2017. Understanding pathways of dissimilatory and assimilatory dissolved inorganic nitrogen uptake in streams. Limnol. Oceanogr. 62 https://doi.org/10.1002/lno.10493.
Rice, E., Association, A, 2012. Standard Methods for the Examination of Water and Wastewater, 22nd ed. American Public Health Association, the American Water Works Association and the Water Environment Federation, Washington D.C.
Schlesinger, W., 2009. On the fate anthropogenic nitrogen. Proc. Natl. Acad. Sci. U. S. A. 106, 203–208. https://doi.org/10.1073/pnas.0810193105.
Seitzinger, S., Harrison, J., Dumont, E.L., Beusen, A., Bouwman, A., 2005. Sources and delivery of carbon, nitrogen, and phosphorus to the coastal zone: an overview of global nutrient export from watersheds (NEWS) models and their application. Glob. Biogeochem. Cycles 19. https://doi.org/10.1029/2005GB002606. GB4S01.
Seitzinger, S., Harrison, J., Bohlke, J., Bouwman, A., Lowrance, R., Peterson, B., Tobias, C., Drecht, G., 2007. Denitrification across landscapes and waterscapes: asynthesis. Ecol. Appl. 16, 2064–2090. https://doi.org/10.1890/1051-0761(2006)016[2064:DALAWA]2.0.CO;2.
Soto, D., Koehler, G., Wassenaar, L., Hobson, K., 2018. Spatio-temporal variation of nitrate sources to Lake Winnipeg using N and O isotope ($\delta^{15}N$, $\delta^{18}O$) analyses. Sci. Total Environ. 647, 486–493. https://doi.org/10.1016/j.scitotenv.2018.07.346.
Spitzy, A., Ittekkot, V., 1991. Dissolved and particulate organic matter in rivers. In: Mantoura, R.F.C., Martin, J.M., Wollast, R. (Eds.), Ocean Margin Processes in Global Change. John Wiley and Sons Ltd, NY, pp. 5–17.
Sun, H., Han, J., Zhang, S., Lu, X., 2015. Carbon isotopic evidence for transformation of DIC to POC in the lower Xijiang River, SE China. Quat. Int. 380–381, 288–296. https://doi.org/10.1016/j.quaint.2015.01.018.
Telmer, K., Veizer, J., 1999. Carbon fluxes, pCO_2 and substrate weathering in a large northern river basin, Canada: carbon isotope perspectives. Chem. Geol. 159, 61–86. https://doi.org/10.1016/S0009-2541(99)00034-0.
Tobias, C., Bohlke, J., 2011. Biological and geochemical controls on Diel dissolved inorganic carbon cycling in a low-order agricultural stream: implications for reach scales and beyond. Chem. Geol. 283, 18–30. https://doi.org/10.1016/j.chemgeo.2010.12.012.
Trimmer, M., Grey, J., Heppell, C., Hildrew, A., Lansdown, K., Stahl, J., Yvon-Durocher, G., 2012. River bed carbon and nitrogen cycling: state of play and some new directions. Sci. Total Environ. 434, 143–158. https://doi.org/10.1016/j.scitotenv.2011.10.074.
Wang, W., Yu, Z., Wu, Z., Song, S., Song, X., Yuan, Y., Cao, X., 2018. Rates of nitrification and nitrate assimilation in the Changjiang River estuary and adjacent waters based on the nitrogen isotope dilution method. Cont. Shelf Res. 163. https://doi.org/10.1016/j.csr.2018.04.014.
Waterson, E.J., Canuel, E.A., 2008. Sources of sedimentary organic matter in the Mississippi River and adjacent Gulf of Mexico as revealed by lipid biomarker and $\delta^{13}C_{TOC}$ analyses. Org. Geochem. 39, 422–439. https://doi.org/10.1016/j.orggeochem.2008.01.011.
Wen, Z., Song, K., Liu, G., Lyu, L., Shang, Y., Fang, C., Du, J., 2020. Characterizing DOC sources in China's Haihe River basin using spectroscopy and stable carbon isotopes. Environ. Pollut. 258, 113684. https://doi.org/10.1016/j.envpol.2019.113684.
Wigley, T.M.L., 1977. WATSPEC: a computer program for determining the equilibrium speciation of aqueous solutions. Bri. Geomorphol. Res. Group Tech. Bull. 20.
Xu, S., Kang, P., Sun, Y., 2016. A stable isotope approach and its application for identifying nitrate source and transformation process in water. Environ. Sci. Pollut. Res. 23, 1133–1148. https://doi.org/10.1007/s11356-015-5309-6.
Xuan, Y., Tang, C., Cao, Y., Li, R., Jiang, T., 2019. Isotopic evidence for seasonal and long-term C and N cycling in a subtropical basin of southern China. J. Hydrol. 577, 123926. https://doi.org/10.1016/j.jhydrol.2019.123926.
Xue, D., Botte, J., De Baets, B., Accoe, F., Nestler, A., Taylor, P., Van Cleemput, O., Berglund, M., Boeckx, P., 2009. Present limitations and future prospects of stable isotope methods for nitrate source identification in surface- and groundwater. Water Res. 43, 1159–1170. https://doi.org/10.1016/j.watres.2008.12.048.
Yang, C., Telmer, K., Veizer, J., 1996. Chemical dynamics of the "St. Lawrence" riverine system: δD_{H2O}, $\delta^{18}O_{H2O}$, $\delta^{13}C_{DIC}$, $\delta^{34}S_{sulfate}$, and dissolved $^{87}Sr/^{86}Sr$. Geochim. Cosmochim. Acta 60, 851–866. https://doi.org/10.1016/0016-7037(95)00445-9.
Yang, M., Liu, Z., Sun, H., Yang, R., Chen, B., 2016. Organic carbon source tracing and DIC fertilization effect in the Pearl River: insights from lipid biomarker and geochemical analysis. Appl. Geochem. 73, 132–141. https://doi.org/10.1016/j.apgeochem.2016.08.008.
Zeng, S., Liu, H., Liu, Z., Kaufmann, G., Zeng, Q., Chen, B., 2019. Seasonal and diurnal variations in DIC, NO_3^- and TOC concentrations in spring-pond ecosystems under different land-uses at the Shawan Karst Test Site, SW China: carbon limitation of aquatic photosynthesis. J. Hydrol. 574, 811–821. https://doi.org/10.1016/j.jhydrol.2019.04.090.
Zhang, J., Quay, P.D., Wilbur, D.O., 1995. Carbon isotope fractionation during gas-water exchange and dissolution of CO_2. Geochim. Cosmochim. Acta 59, 107–114. https://doi.org/10.1016/0016-7037(95)91550-D.
Zhao, H., Xiao, Q., Miao, Y., Wang, Z., Wang, Q., 2020a. Sources and transformations of nitrate constrained by nitrate isotopes and Bayesian model in karst surface water, Guilin, Southwest China. Environ. Sci. Pollut. Res. https://doi.org/10.1007/s11356-020-08612-8.
Zhao, H., Xiao, Q., Zhang, C., Zhang, Q., Wu, X., Yu, S., Miao, Y., Wang, Q., 2020b. Transformation of DIC into POC in a karst river system: evidence from $\delta^{13}C_{DIC}$ and $\delta^{13}C_{POC}$ in Lijiang, Southwest China. Environ. Earth Sci. 79, 295. https://doi.org/10.1007/s12665-020-09039-7.